applied sciences

MDPI

Article

Research on the Indoor Thermal Environment of Attached Sunspace Passive Solar Heating System Based on Zero-State Response Control Strategy

Jing Zhao, Dehan Liu and Shilei Lu *

Tianjin Key Laboratory of Built Environment and Energy Application, School of Environmental Science and Engineering, Tianjin University, Tianjin 300072, China; zhaojing@tju.edu.cn (J.Z.); liudehan@tju.edu.cn (D.L.)
* Correspondence: lvshilei@tju.edu.cn

Featured Application: In cold climatic zones of China, an attached sunspace passive solar heating system was installed on a farmhouse to improve the indoor thermal environment in winter.

Abstract: The application of attached sunspace passive solar heating systems (ASPSHS) for farmhouses can improve building performance, reduce heating energy consumption and carbon dioxide emissions. In order to take better use of the attached sunspace to prevent heat transfer or promote natural ventilation, this paper presented a zero-state response control strategy for the opening and closing time of active interior window in the ASPSHS. In order to verify the application of this strategy, an attached sunspace was built in an actual farmhouse. A natural ventilation heat exchange model was built based on the farmhouse with attached sunspace. The proposed zero-state response control strategy was implemented in TRNSYS software. Field measurement in living lab was carried out to inspect the distribution of the thermal environment in the farmhouse with attached sunspace under a zero-state response control strategy in the cold region of northern China. The experimental results show that, even under −5.0–2.5 °C ambient temperature, the application of zero-state response control strategy effectively increases the internal temperature to an average of 25.45 °C higher than the outside, with 23% indoor discernible temperature differential in the sample daytime. The whole-season heating performance was evaluated by simulating the model for the heating season in 2020–2021. The simulation demonstrates that the ASPSHS under zero-state response control strategy can maintain a basic indoor temperature of 14 °C for 1094 h during the heating season, with a daytime heating guarantee rate of 73.33%, thus ensuring higher indoor heating comfort during the day. When compared to a farmhouse with an attached sunspace under the zero-state response control strategy, the energy savings rate can be enhanced by 20.88%, and carbon emissions can be reduced by 51.73%. Overall, the attached sunspace with the zero-state response control strategy can effectively increase the indoor temperature when the solar radiation is intensive and create a suitable thermal environment for the farmhouse in the cold region of northern China.

Keywords: attached sunspace passive solar heating systems; energy consumption; indoor thermal environment; zero-state response control strategy

check for updates

Citation: Zhao, J.; Liu, D.; Lu, S. Research on the Indoor Thermal Environment of Attached Sunspace Passive Solar Heating System Based on Zero-State Response Control Strategy. *Appl. Sci.* **2022**, *12*, 855. https://doi.org/10.3390/app12020855

Academic Editor: Luisa F. Cabeza

Received: 20 November 2021
Accepted: 11 January 2022
Published: 14 January 2022

Publisher's Note: MDPI stays neutral with regard to jurisdictional claims in published maps and institutional affiliations.

Copyright: © 2022 by the authors. Licensee MDPI, Basel, Switzerland. This article is an open access article distributed under the terms and conditions of the Creative Commons Attribution (CC BY) license (https://creativecommons.org/licenses/by/4.0/).

1. Introduction

Accelerating the promotion of low-carbon and energy-saving buildings has become the dominant development trend in the construction field, as proposed by China's aim of "carbon peaking and carbon neutralization" [1,2]. The utilization of passive solar energy and energy-saving design solutions in cold climates can greatly cut winter heating energy use [3]. In the winter, the climate in northern China is chilly, and residents have a strong desire to improve their temperature in their homes. The favorable sunshine conditions in the countryside along with rural houses being mostly low-rise buildings with low density

make it suitable for the development of passive solar heating technology [4]. Therefore, a suitable construction of passive solar heating systems (PSHS) for new constructions or reconstructions of existing farmhouse buildings in northern China has tremendous energy-saving renovation potential for reducing energy consumption in winter heating [5].

Currently, research on PSHS is mostly focused on Trombe walls, direct-gain room, and attached sunspace and other types of solar room [6]. Trombe walls have been investigated by several experts over the last few decades as an essential passive solar heating device. Wang et al. [7] analyzed Trombe walls' classification, testing, modeling, and evaluation. Trombe walls' heat storage and thermal resistance performance have been much enhanced thanks to advances in material technology, particularly the use of heat storage materials and aerogel materials. However, due to its structure, it combines absorption, heat storage, heat release and less internal air buffering, which leads to insufficient thermal resistance, and losses of significant quantities of heat to the outside during its operation are inevitable.

The direct-gain room, as the most basic PSHS model, offers the advantages of a simple design and inexpensive cost. However, because of its single adjustment mechanism and weak heat storage efficiency, it is prone to glare and significant indoor temperature swings when in operation. Si et al. [8] proposed a new double-layer transparent enclosure structure with changeable thermal resistance that uses a step control operating technique. This design and control method increase this type of PSHS's controllable performance and solar energy collecting, allowing the indoor air temperature to be further increased. Gong et al. [9] proposed a novel type of solar house integrated with flat gravity-assisted heat pipes. Single-direction heat transfer in buildings effectively improves the solar energy absorption rate, wall heat storage rate and indoor temperature of the room. However, the above-mentioned scholars used clever design and control methods to improve the shortcomings of this type of PSHS, and the heat gain brought by the PSHS has been further improved. Due to problems with the layout, there are natural deficiencies in thermal resistance, heat storage and solar heat collection areas, and excessive optimization has diluted the cost-cutting benefits.

The ASPSHS is a mixed deformation of Trombe walls and direct-gain room. The problem of insufficient heat collection during the day of the direct-gain room and insufficient air thermal resistance of the Trombe wall at night can be overcome by building a large-volume glass room on the south side of the room [10,11]. During the daytime, the attached sunspace is employed as a heat collecting component to raise the internal air temperature by absorbing solar radiation heat, and storing part of the heat to the wall and transmission into the room. The effects of the attached sunspace on the indoor thermal environment can be classified into two modes: when the active interior window is opened, the natural air convection between the attached sunspace and room is delivering; when the active interior window is closed, the air in the attached sunspace forms an insulation to prevent heat transfer. Therefore, influence of the attached sunspace on the indoor thermal environment can be regulated by controlling the opening and closing status of the interior active window. In order to further improve the performance of the ASPSHS, scientists from various countries have conducted research on different aspects. Liu et al. [12] carried out ASPSHS transformation on a farm house in Qinghai. The results of the experiments revealed that improving maintenance structure performance can reduce the amount of auxiliary heat source (coal burning), improve indoor thermal comfort and decrease indoor pollution; Wang et al. [13] conducted experiments and simulation by placing an attached sunspace on the roof with various design parameters considered. The results demonstrate the benefit of using an attached sunspace to reduce heating energy consumption in farmhouses in China's cold regions; Ma et al. [14] used EnergyPlus software to model the glass unit of the attached sunspace in a farmhouse in northeast China. The simulated results showed that an attached sunspace's double-glazed units with a 9 mm krypton layer in cold regions provides the greatest energy savings; Lu et al. [15] and Li et al. [16] used PCM radiant floor and PCM louvers, respectively, to improve an attached sunspace's heat storage

effect, demonstrating that combining the attached sunspace with reasonable phase change materials can significantly improve the heating and energy-savings effect of buildings.

Current research focuses mostly on the optimizing and enhancing the thermal insulation and heat storage qualities of its envelopes [10–16]; there is little research on the indoor heating methods of attached sunspaces, which could not have an impact on this modifiable state nor is the dynamic indoor environment enhanced. In order to better take advantage of the two effects of ASPSHS on the indoor thermal environment, this paper proposes a new strategy, which can better adjust the opening and closing time of the interior active window. Attached sunspace and indoor natural ventilation heat exchange were modeled to simulate the strategy, and the dynamic distribution of the thermal environment was obtained by field measurement.

2. Methodology

In this paper, an attached sunspace was built in an actual farmhouse located in Tianjin's Ninghe District, China, which was used as a living lab for the zero-state response control strategy. In order to obtain more efficiency in the control strategy of the interior active window, the attached sunspace and indoor natural ventilation heat exchange were modeled by TRNSYS, which was validated in the living lab experiment. The distribution of the thermal environment was measured and compared at different points of time during the operation. Furthermore, this model simulation for the whole heating season was performed to comprehensively evaluate the all-season heating performance.

2.1. Layout of the Farmhouse

The living lab is in Tianjin's Ninghe District, at 117°22′32″ east longitude and 39°19′3″ north latitude, which are a typical representative city in the cold area of northern China, and the calculated heating time is 118 days. The outdoor temperature and solar radiation intensity during the heating season from 1 November 2020 to 28 February 2021 are shown in Figure 1.

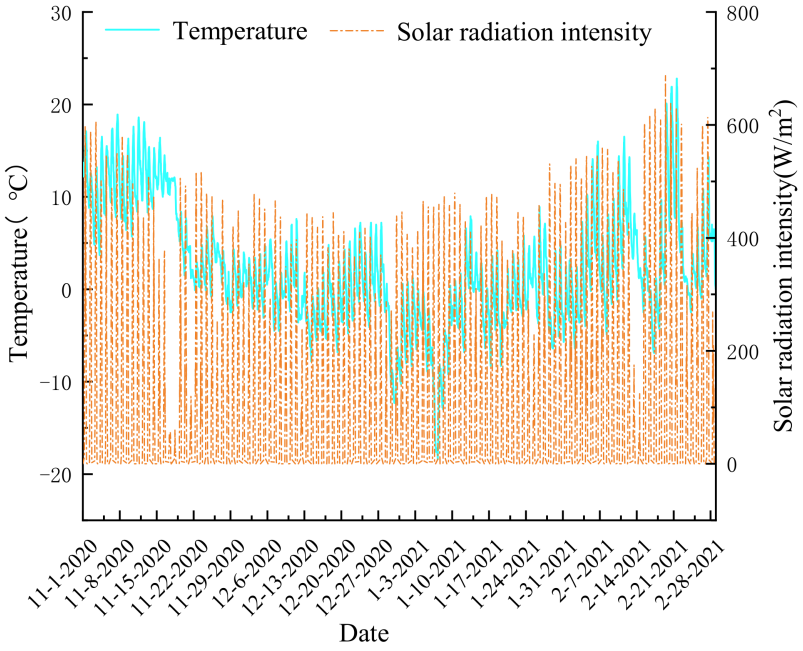


Figure 1. Outdoor weather conditions from 1 November 2020 to 28 February 2021.

As shown in Figure 1, the coldest month in this location is January, which has an average temperature of −2.9 °C. The number of sunlight hours is 178.4 h, the sunshine guarantee rate is 24.78% and the average solar radiation is 224.95 W/m^2. Although the

outdoor temperature is relatively low, solar energy resources are quite abundant, which is a better place for the application and development of passive solar structures [17].

The farmhouse for this research was built in the 1980s and is a traditional single-story brick-concrete rural building in northern China. Figure 2 depicts the farmhouse's structural schematic. The farmhouse faces 11° west-south, and the south facade is clear, with enough sunlight space between the other buildings. Bedroom 2 is the experimental room for the living lab. The dimensions of the room are 4.36 m long, 3.00 m wide and 2.65 m high. An attached sunspace has been developed on the south side of the space, unlike the other room. The appearance of the living lab is shown in Figure 3.

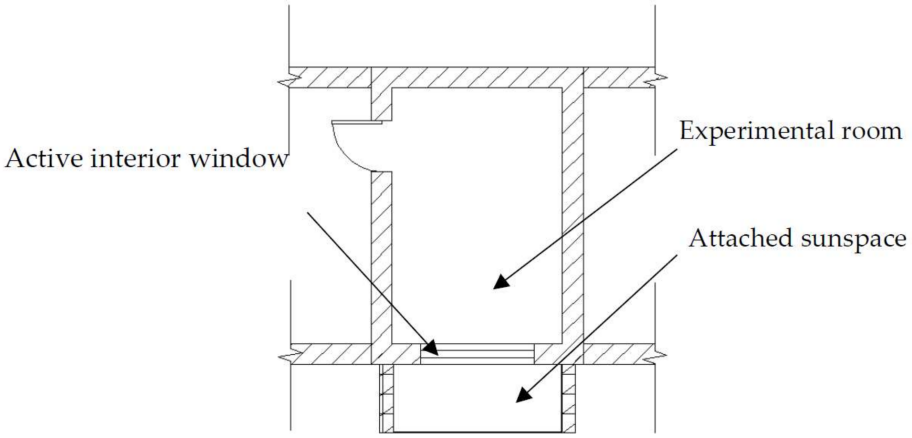


Figure 2. Structural schematic of the living lab.



Figure 3. Real view of the farmhouse with attached sunspace.

Due to poor thermal performance of the original enclosure structure, its envelope structure has undergone internal thermal insulation transformation. The roof is a 20° tile roof + 60 mm thick EPS board ceiling; the ground is 60 mm thick EPS board + 10 mm concrete + ceramic floor; the east and west interior walls are 240 mm thick brick walls + 60 mm EPS board; the north exterior wall and the south public wall are both 370 mm thick brick walls + 60 mm EPS plate. The public wall's windows are 5 + 22 + 5 double-layer hollow glass, the solar radiation transmittance of this kind of glass is more than 80%. And the windows' skeleton uses 70 series bridge-cutoff aluminum alloys with size of 2.00 m × 1.50 m. There are 0.60 m × 1.00 m flat active interior window in the west and the remainder are fixed windows [18]. The heat transfer coefficient of the envelope structure before and after the transformation is shown in Table 1.

Table 1. The thermal resistance of the envelope structure before and after the transformation.

Building Envelope	Heat Transfer Coefficient after Transformation W/(m^2·K)	Heat Transfer Coefficient before Transformation W/(m^2·K)
Roof	0.301	1.56
Ground	0.35	0.5
Exterior wall	0.34	1.53
Interior wall	0.44	2.03
Windows	1.448	4.4

The attached sunspace has a depth of 1.2 m, a width of 2.0 m, an 8-degree roof slope, and a height of 2.5 m on the south facade. The ground is 270 mm red brick + cement; on the east and west sides, there are 250 mm thick brick walls with gray cement coating, with a heat transfer coefficient of 1.10 W/(m^2·K); the south facade and top are 5 + 22 + 5 double-layer hollow glass with 70 series bridge-cutoff aluminum alloy as the skeleton, with a heat transfer coefficient of 1.448 W/(m^2·K).

2.2. Experimental Setup

During field experiments, the experimental material mostly consisted of collecting exterior side parameters, the attached sunspace's parameters and internal parameters of the farmhouse [19]. The detailed information of measurement instruments can be seen in Table 2.

Table 2. Details of measurement instruments.

Test Instrument	Rang	Accuracy
HOBO Portable Weather Station	0~1280 W/m^2	±10 W/m^2
	−40~+75 °C	±0.21 °C
HOBO Recorder of Temperature and Humidity	20~70 °C	±0.21 °C
	15–95%	±3.5%
TR004 Temperature Recorder	−30~125 °C	±0.5 °C
TNL-3RLTemperature and Heat Flow Monitoring System	−500~500 W/m^2	±5%

The following parameters were measured in the experiment:

(1) Outdoor side parameters: the portable weather station were used to measure outdoor temperature, humidity and solar radiation strength. The measuring points were located on the room's roof.

(2) Attached sunspace parameters: the heat flow meters were used to measure the heat flow of the heat storage partition wall, and the temperature and humidity recorders were used to measure the temperature and humidity of the air layer. Figure 4a shows the configuration of the measuring points.

(3) Indoor side parameters: the temperature and humidity recorder was used to measure the indoor temperature and humidity. Figure 4b shows the configuration of the measuring points.

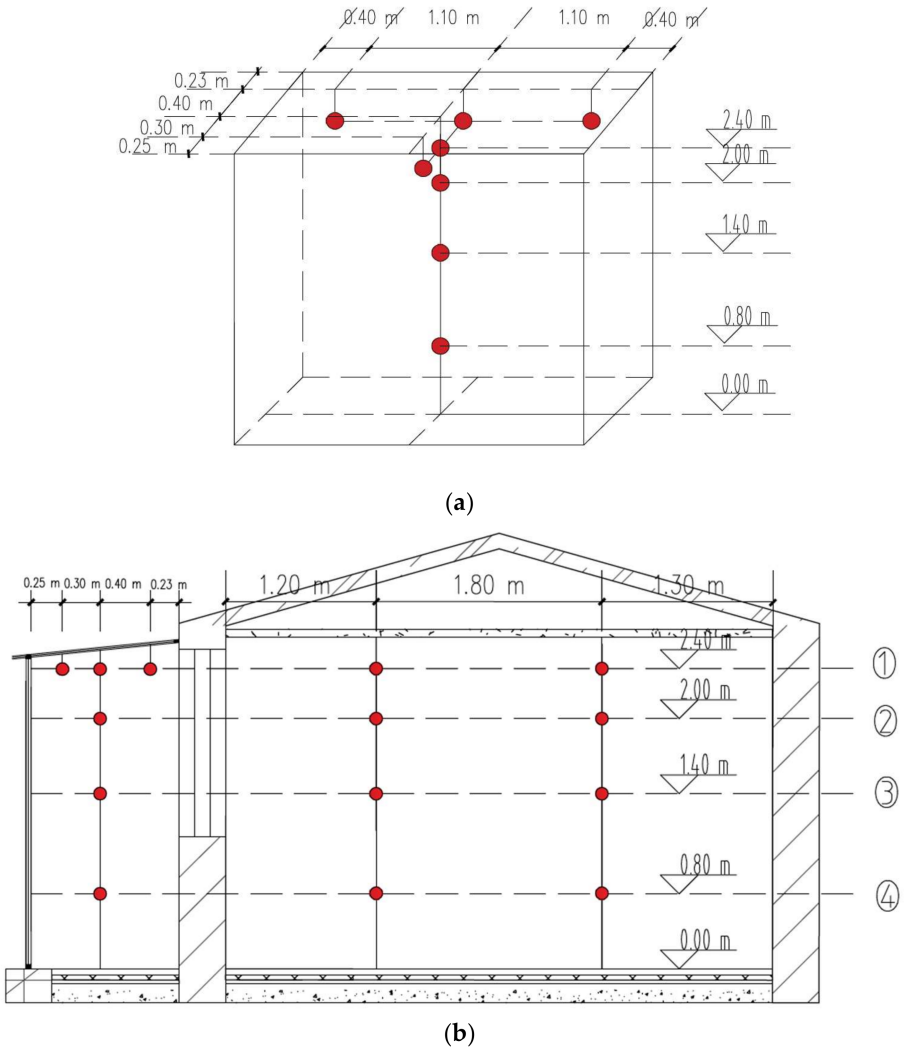


Figure 4. Layout of measuring points in the living lab: (**a**) Layout of measuring points in the attached sunspace; (**b**) Layout of measuring points of the interior.

2.3. System Modeling

2.3.1. TRNSYS Model

Natural ventilation heat exchange through an active interior window is dependent on the pressure difference between the attached sunspace and indoor and the effective opening area of windows. This model only considers the buoyancy-driven ventilation [20]. It arises due to density differences of the indoor and attached sunspace's air. The density of warmer air is lower than the density of colder air and tends to rise above the cold air [21]. The maximum potential air change (ACRmax.pot) is defined by Equation (1).

$$ACR_{max.pot} = \eta \frac{A_{top}}{V} 9.81 H \sqrt{\left(\frac{\left|T_{air.room} - T_{air.sunspace}\right|}{T_{air.sunspace} + 273.15}\right)\left(\frac{{A_{top}}^2 + {A_{bot}}^2}{{A_{bot}}^2}\right)} \quad (1)$$

where η denotes the stack effect efficiency; A_{top} denotes the upper opening area, m^2; A_{bot} denotes the lower opening area, m^2; H denotes height between the openings, m; $T_{air.room}$ denotes the room air temperature, °C; $T_{air.sunspace}$ denotes the sunspace air temperature, °C.

TRNSYS (transient system simulation program) is a program that simulates energy systems (particularly building energy systems) and other dynamic systems. It is now widely utilized by engineers all over the world in low-energy buildings, HVAC system design optimization, renewable energy (such as wind energy and solar hydrogen) system design

optimization and other applications. It is particularly useful for solar system simulation research. Therefore, TRNSYS software is used to simulate the natural ventilation heat exchange model [22].

The natural ventilation heat exchange model in TRNSYS is primarily made up of three modules: the building module, natural ventilation control module and weather reading module, as shown in Figure 5. Through TRNBuild, the building module is modeled based on the current circumstances, the natural ventilation module is used to mimic natural ventilation in the attached sunspace and inside the building, and the weather module is used to read the current weather parameters [23]. Considering that the weather changes usually take an hour to change significantly, time step sets as one hour in the simulation process [8].

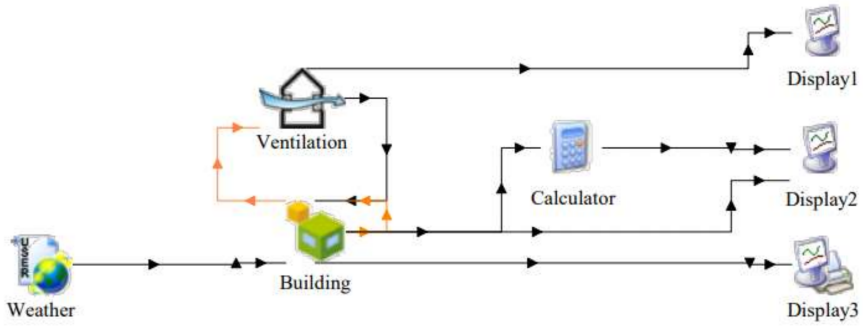


Figure 5. System model diagram of TRNSYS.

2.3.2. Model Verification

In order to verify the accuracy of the TRNSYS model, the temperature change of the attached sunspace and inside was simulated when the active interior window was not opened from 00:00 to 23:00 on 18 December 2020; the simulated parameters are based on the actual meteorological parameters. Meanwhile, the simulation results were compared with the average temperature of the attached sunspace and indoors obtained from the actual measure on 18 December 2020. Figure 6 depicts the comparison of outcomes:

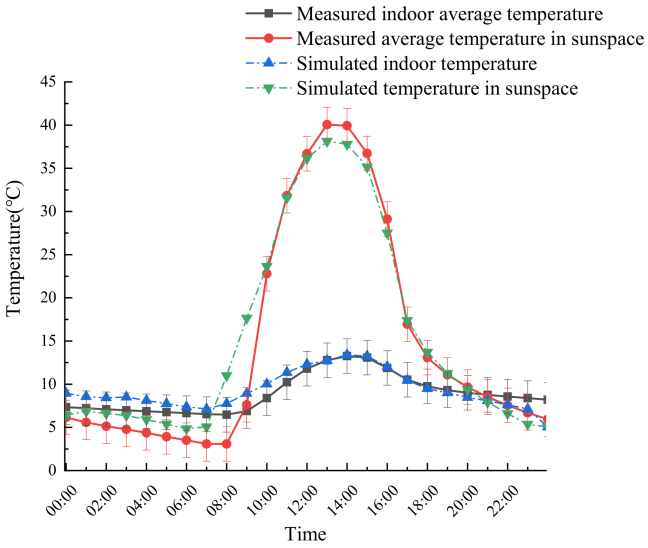


Figure 6. The comparison of simulated and measured temperature.

When the interior active window was not opened on 18 December 2020, as shown in Figure 6, the measured value was nearly identical to the calculated value. The primary

inaccuracy occurring between 00:00 and 10:00, which is because the simulation ignores the heat radiated through the glass, resulted in a simulated night temperature that is higher than the measured value. The normalized mean bias error (*NMBE*) proposed by ASHRAE guideline14-2014 [24] were selected to evaluate the accuracy of the forecasted results, and the formulas are shown in Equation (2).

$$NMBE = \frac{\sum_i^n |T_{sim} - T_{mea}|}{n\overline{T_{mea}}} \times 100 \quad (2)$$

where, T_{sim} denotes the simulated temperature and °C; T_{mea} denotes the measured temperature, °C.

According to calculations, the average relative errors of the experimental and simulated values of the average temperature in the attached sunspace and indoor area were 9.04% and 11.14%, respectively. Compared with the standard reference of 10%, the mistakes are minor and the accuracy of the TRNSYS model and simulation method may be demonstrated.

3. Results

3.1. Zero-State Response Control Strategies

In the daytime, the attached sunspace is used as a heat collection component, which increases the internal air temperature by absorbing solar radiation, and stores part of the heat in the envelope structure. When the active window is opened, it can promote the convection of the attached sunspace and the indoor air under the effect of temperature difference. In the nighttime, due to the favorable tightness and heat preservation of the attached sunspace, the internal air heat dissipates slowly to the outside, which provides an extra layer of air insulation for the room. Therefore, the attached sunspace has a different mechanism of action on the room during the day and night, and different control strategies are adopted for the opening and closing of the active window. The zero-state response control strategy was provided to adjust the two states of active interior window:

1. Zero-state: if the temperature of the attached sunspace is lower than the room, the active interior window is at the closed state and prevents air flow through the windows.
2. Response-state: if the temperature of the attached sunspace is higher than the room, the interior active window is in the opened state and delivers air flow through the windows.

In order to obtain more efficiency of the strategy, a determined opening and closing time of the interior active window was simulated by TRNSYS.

3.1.1. Opening Time at Morning

As the intensity of solar radiation rises, the temperature of the attached sunspace increases in the morning, resulting in a thermal pressure difference with the lower indoor temperature. When the interior active window on the public wall is opened, the attached sunspace's high-temperature air heats the room by thermal convection. In order to establish the ideal opening time of the interior active window, this article evaluates the attached sunspace's heating impacts at different opening times based on TRNSYS model. The simulation results can be seen in Figure 7.

As Figure 7 shows, the influence of the different window opening time on the indoor temperature is primarily focused on the pace of increase in heating start. Nevertheless, it has little effect on the temperature once the heat exchange has stabilized. In the absence of solar radiation, indoor and attached sunspace's temperatures are steadily dropping. When solar radiation begins to intensify, the temperature of attached sunspace progressively rises. Despite that the indoor temperature's rate of decrease has slowed, the decline will continue until the temperature of the attached sunspace is higher than the indoor temperature. When the interior active window is not opened, the indoor temperature rises at a relatively slow rate, due to the indoor environment receiving the sunlight radiation from the closed

window and the heat conducted through the public wall. However, when the interior active window is opened, natural convection brings the heated air from the sunspace into the room and the indoor temperature rises rapidly.

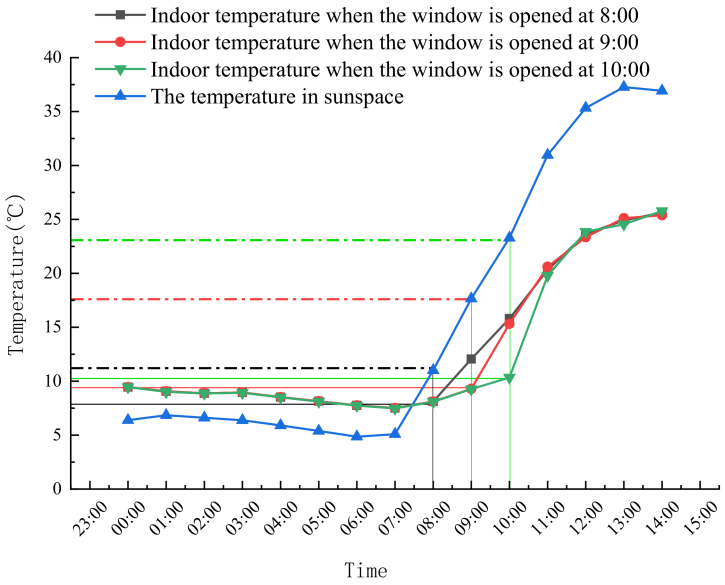


Figure 7. The temperature comparison for different window opening time.

When comparing the inside temperature curves at various opening times, the difference is noticeable. The earlier the interior active window is opened, the higher the average indoor temperature at the initial moment, and the later the window is opened, the faster the indoor temperature rate rises. The main reason for this phenomenon is that under the solar radiation, the heat gain in the sunspace is much greater than indoor, and the thermal resistance caused by the closing of the interior active window makes the indoor temperature increase at a much lower rate. As a result, this temperature difference grows greater and larger in the morning as time passes, and the later the window is opened, the greater the heat pressure. This reason caused the faster indoor temperature increases. However, because of the heat transfer balance, the internal temperature remained constant regardless of when the window was opened.

In conclusion, when the interior active window is opened earlier, due to the lower temperature of the attached sunspace, the temperature difference between the room at this time is small, and the natural convection heating effect formed is also limited. In order to make the natural convection more effective, the actual control strategy should allow the interior active window when there is a temperature of attached sunspace higher by 10 °C than indoors. In this simulation, the best opening time is around 10:00.

3.1.2. Closing Time at Dusk

As the solar radiation diminishes, the heat collected by the attached sunspace is insufficient to maintain the thermal environment. The closing of the interior active window is conducive to increasing the thermal resistance of the farmhouse, but it also weakens the heat transfer from the attached sunspace to the room. When the interior active window is closed at different times, the indoor temperature also exhibits a different rate of decrease. In order to obtain the optimal closing time, a comparative of the indoor temperature changes at different closing times by simulation, shown in Figure 8.

As shown in Figure 8, the attached sunspace and indoor temperature reach a maximum at 14:00, but then rapidly decreases as solar radiation intensity and outdoor temperature decrease. With the disappearance of solar radiation after 17:00, the decline rate of the attached sunspace and indoor temperature slowed due to the small temperature difference

between indoor and outdoor. When the window was closed between 14:00 and 17:00, the indoor temperature dropped dramatically. This result shows that, the closing of the interior active window prevents the heat of the attached sunspace entering the room, and the earlier closing of the windows is not conducive to maintaining the room thermal environment. Without the heat transfer from the attached sunspace to the room, the indoor temperature will drop dramatically due to the interior air loses its main heat source and the leftover heat is transferred to the outside through the enclosure construction. Furthermore, the earlier the interior active window closes, the lower the average indoor temperature. However, if the later window closing time for the attached sunspace's temperature is lower, there is not enough temperature difference to provide power for natural convection and the heating effect is limited. Therefore, the best time to close the windows in this simulation should be around 17:00, which is more beneficial to maintain the heat in the room.

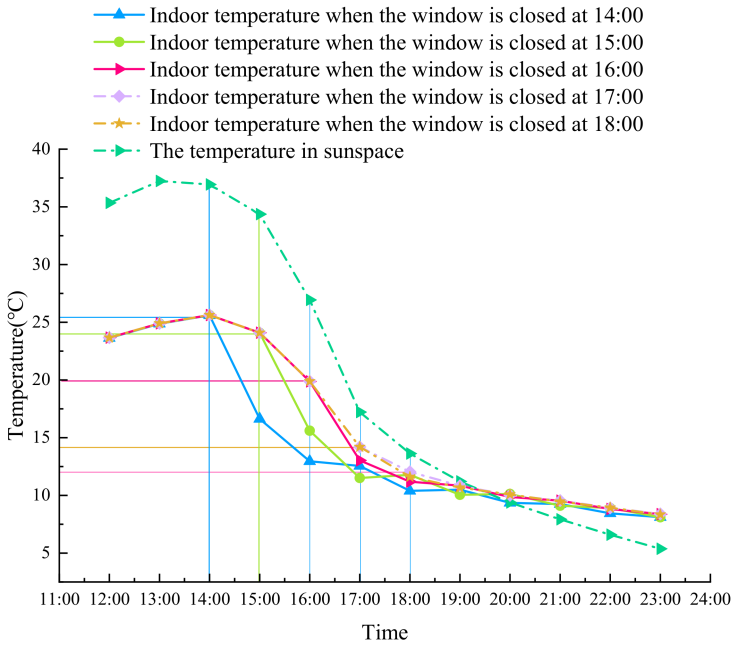


Figure 8. Temperature comparison chart for different window closing times.

3.2. Daytime Thermal Environments

In order to test and evaluate the indoor thermal environment distribution with the change of daytime under the zero-state response control strategy, a representative day was chosen for the actual measurement experiment in the living lab.

3.2.1. Choice of Sample Day

In order to test the operation effect of the optimized dynamic heat transfer process, a sample day should be identified for the actual measurement experiment in the living lab. Figure 9 shows the weather changes during the time of the experiment.

As shown in Figure 9, the solar room's heat collecting effect is limited due to the low solar radiation intensity, and the external temperature is too high to show its role. The average daytime temperature on 28 January was −3.68 °C, which was one of the coldest days during this period. The maximum solar radiation intensity was 560.6 W/m^2, which is at the median value for this period. Therefore, day of 18 January was chosen as representative for the experiment.

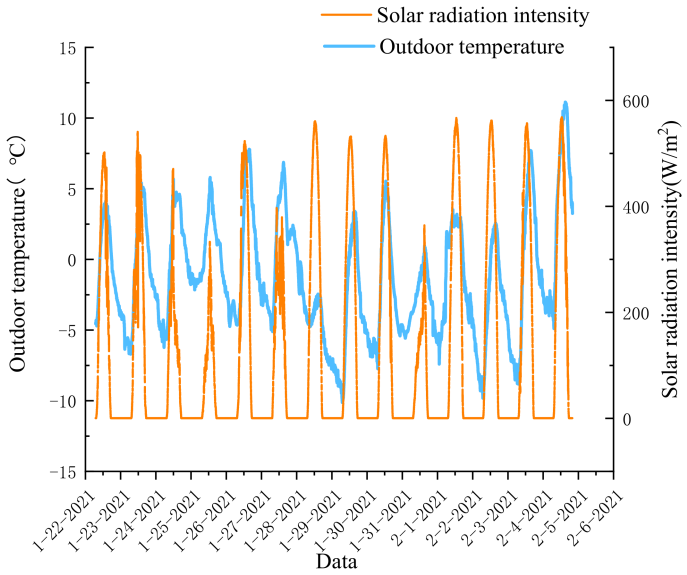


Figure 9. The weather changes during the time of the experiment.

3.2.2. Temperature of Room under Zero-State Response Control Strategy

In order to verify the heat collection and heating effect of the attached sunspace under the zero-state response control strategy, the actual test was conducted for the experimental room. The changes in the attached sunspace temperature and indoor temperature with outdoor temperature and solar radiation intensity are shown in Figure 10.

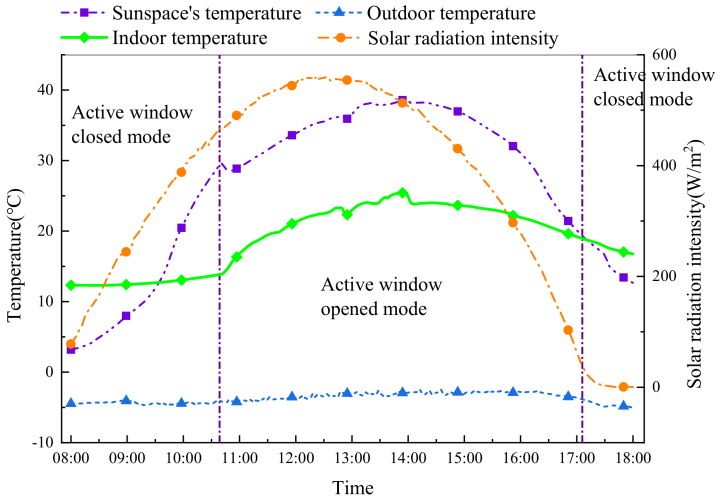


Figure 10. Temperature of room under zero-state response control strategy on 28 January.

The temperature of rooms under zero-state response control strategy on 28 January is shown in Figure 10. With the change of solar radiation and the attached sunspace's temperature, the opening time of the active interior window was selected at 10:40, the temperature difference was higher than 10 °C at this time; the closing of the active interior window was selected at 17:10, the temperature of the attached sunspace was the same as the indoor space at this time.

Despite the sun radiation is intense in daytime, the outdoor temperature is as low as only reaching −5.0–2.5 °C. On the other hand, the indoor environment is always at a greater temperature under the zero-state response control strategy. Prior to 10:40 a.m., the temperature of the sunspace will gradually rise owing to solar radiation, but the indoor temperature will not vary dramatically due to the enhanced thermal resistance of the closed

window. Only part of the heat through the public wall heats the room. Between 10:40 and 17:10, opening the interior active window stimulates the convection heat exchange and raises the indoor temperature. The average indoor temperature is 21.69 °C, and rose to 25.07 °C higher than outdoor. The greatest temperature was reached at 14:00, which is 25.45 °C and 28.31 °C higher than outdoor. After 17:10, the interior active window was closed, increasing the room's thermal resistance, which helped to slow down the loss of inside heat. Furthermore, due to the heat storage of the envelope construction in the daytime, the rate of decline of the indoor temperature drops slowly.

3.2.3. Attached Sunspace's Thermal Environment

The temperature distribution of the air interlayer is uneven in the attached sunspace due to the large cavity, especially during the process of the solar radiation rising. When the interior active window is opened, the convective heat exchange effect is affected by the distribution of air temperature inside the attached sunspace. Thus, the change of temperature distribution in the attached sunspace was measured after being exposed to the solar radiation.

Figure 11 depicts the thermal environment distribution variation with time of the four longitudinal measuring points at the center of the attached sunspace. As shown in Figure 11a, in order to examine the morning thermal environment longitudinal distribution in the attached sunspace, we investigated the part 0.63 m south of the public wall, which is the longitudinal section where the previously established temperature measurement stations are located. As described in Figure 11b–f, the temperature in the attached sunspace steadily rises from 8:00, and the temperature stratifies from 8:30. Significant temperature stratification occurs at 9:00. The greatest temperature is recorded at point 2, which is 9.71 °C. The temperature of point 1 is lower than that of point 2, which is 7.22 °C, which is because of the closer to the glass roof, the more severe of heat loss. The temperature of lower point 3 and point 4 is 6.92 °C and 4.49 °C, respectively. The heat gain of the attached sunspace increases significantly after 9:30, but the temperature stratification structure is similar to 9:00. At 10:00, the longitudinal average temperature reaches 20.7 °C, while the temperature at point 2 in the upper middle is the greatest and the lower temperatures are top point 1, lower middle point 3 and bottom point 4 in this order.

Figure 12 depicts the thermal environment distribution variation with time of the five transverse measuring sites at the top of the attached sunspace. As showed in Figure 12a, in order to examine the morning thermal environment cross distribution in the attached sunspace, is balanced in the longitudinal distribution due to the top position, a triangular cross section 0.1 m from the roof of the sunspace was investigated, where the previously established temperature measurement stations are located. As described in Figure 12b–f, the air temperature in the attached sunspace's top horizontal plane is essentially the same at 8:00, with the western portion being somewhat higher than the rest. The temperature difference is not evident due to the weak solar radiation. Solar radiation has increased from 8:30, and the temperature in each region starts to climb. Because the solar radiation angle is southeast to northwest, the southern portion of the attached sunspace gains total solar radiation sooner and more than the other locations, resulting in a much higher temperature than the other locations. Due to the western portion being close to the wall, the resulting solar radiation was absorbed by the wall, and the temperature was lower than that in the south area but higher than that in other locations. The east wall blocks solar radiation, and the eastern portion was exposed to solar radiation last, and the temperature can only rely on the air movement inside the sunspace to increase. Therefore, it is always the lowest temperature in the attached sunspace. At 9:30, the temperature remained higher in the southern portion than in the western portion than in the central portion than in the northern portion than in the eastern portion.

In summary, according to our research on the thermal environment of the attached sunspace during the heat collection process, the temperature field is unevenly distributed, and the internal heated air of the attached sunspace is more likely to gather in the upper

middle position of the longitudinal distribution and the west and south position of the cross distribution in the morning. The position of the interior active window that would choose to open is west and in upper section of the public wall, in order to facilitate the heated air entering the room. When the interior active window of this position is opened, the heat pressure created is sufficient to allow sufficient hot air flow to the room and maintain an indoor thermal environment.

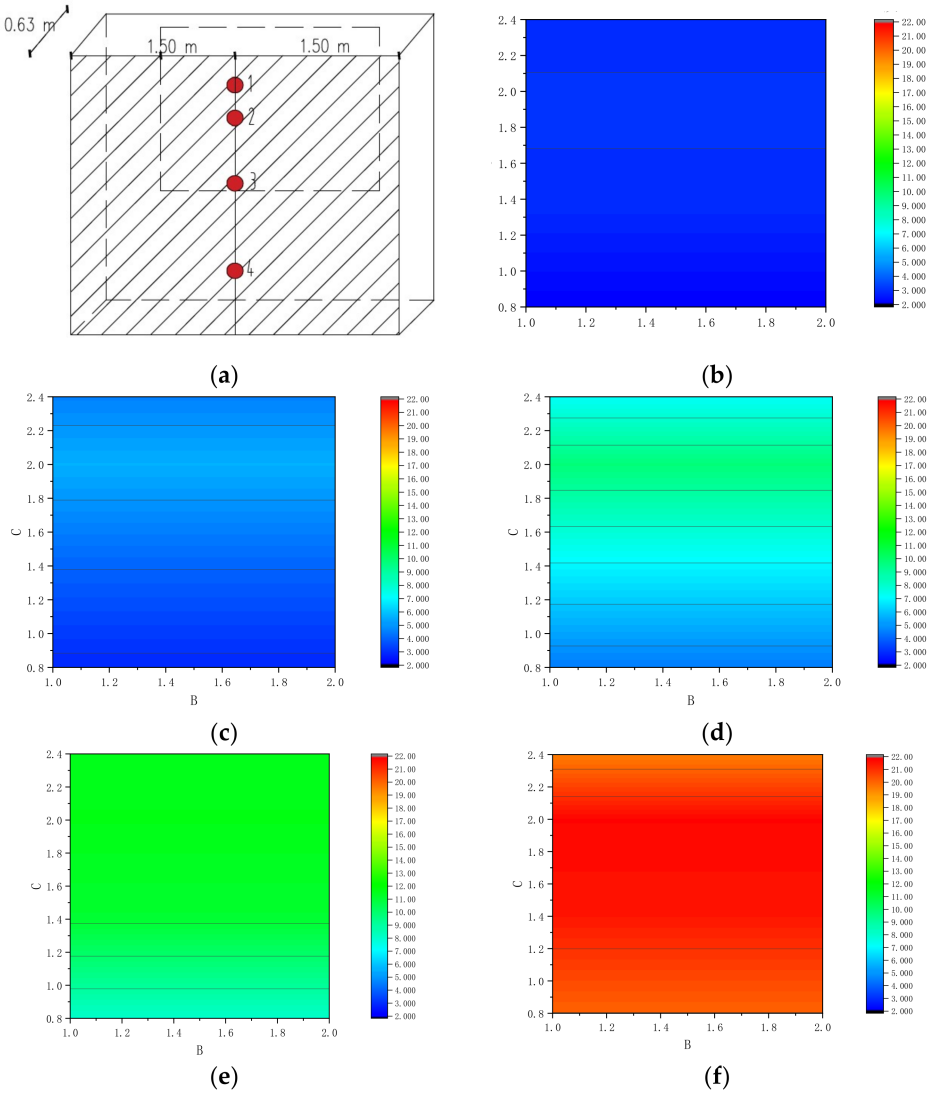


Figure 11. Longitudinal distribution map of the morning sunspace's thermal environment on 28 January; (**a**) Attached sunspace's longitudinal section of temperature field; (**b**) Distribution of temperature field at 8:30; (**c**) Distribution of temperature field at 9:00; (**d**) Distribution of temperature field at 9:30; (**e**) Distribution of temperature field at 10:00; (**f**) Distribution of temperature field at 10:30.

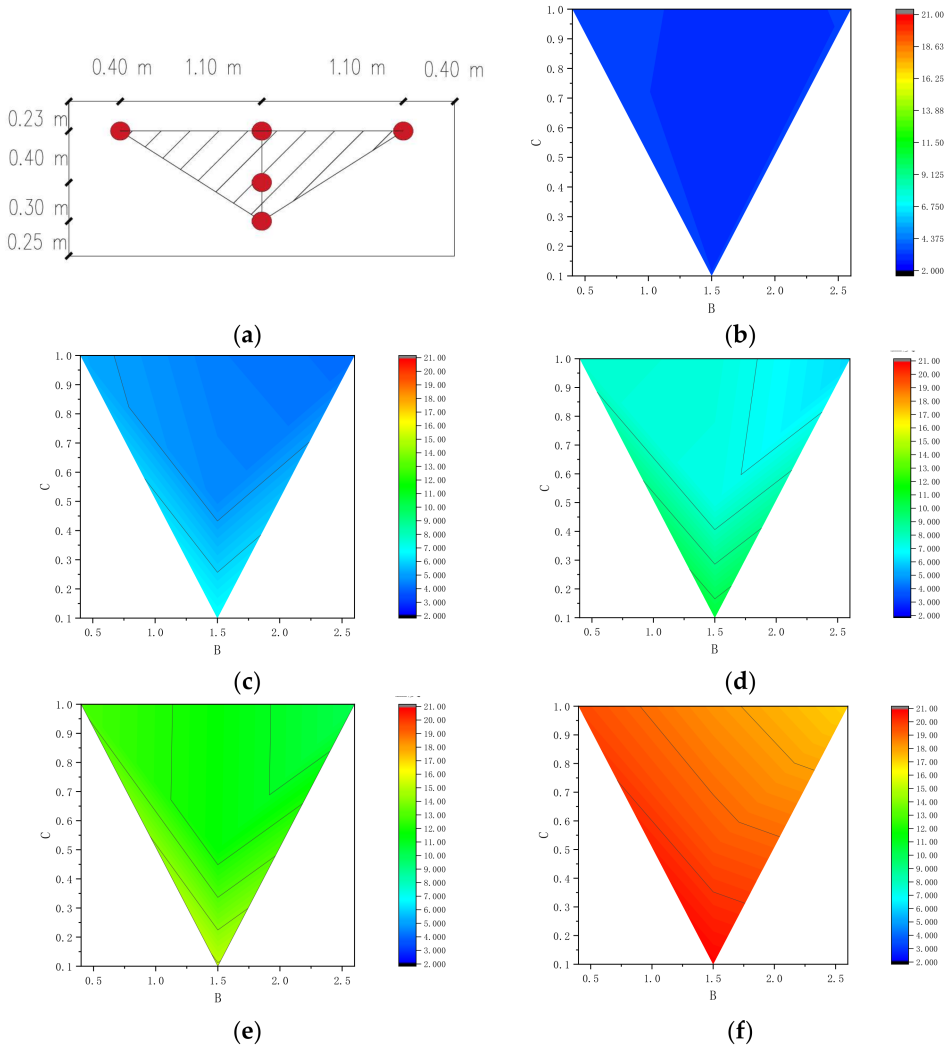


Figure 12. Cross distribution map of morning the sunspace's thermal environment on 28 January; (**a**) Attached sunspace's cross section of temperature field; (**b**) Distribution of temperature field at 8:30; (**c**) Distribution of temperature field at 9:00; (**d**) Distribution of temperature field at 9:30; (**e**) Distribution of temperature field at 10:00; (**f**) Distribution of temperature field at 10:30.

3.2.4. Indoor Thermal Environment

The attached sunspace transmits heat into the room in two ways after the active interior window is opened: heat is transmitted into the room through the active interior window via convection heat exchange at first; afterwards, the outer surface of the public wall absorbs solar radiation, transmits it to the inner surface via heat conduction, and then transmits it to the indoor air via convection. The active interior window was opened at 10:40 and closed at 17:00 on 28 January. Distribution of indoor temperature variation with time of measuring points is depicted in Figure 13.

As shown in Figure 13a, in order to examine the indoor thermal environment tangential distribution on the daytime of 28 January, the longitudinal section in the north-south direction at the center of the room 2 was investigated, which is the longitudinal section where the previously established temperature measurement stations are located. As described in Figure 13b–k, when the active interior window was not opened from 9:00 to 10:00, the temperature in the south of the room was slightly higher than that in the north due to the influence of solar radiation and heat transfer through the public wall, but the indoor temperature remained cold at less than 14 °C. When the interior active window was opened from 11:00 to 15:00, the indoor ambient temperature rose rapidly, and distribution started

to be uneven. Overall, the indoor thermal environment in the south was greater than that in the north and a higher temperature in the upper layer than in the lower. However, the temperature of the lower space in the south of the room, is the most prominently affected by the ASPSHS. The temperature hits 30.93 °C at 14:00, the maximum indoor temperature of the day. But while the temperature at this place began to drop, the temperature in other locations impacted by thermal convection continued to rise. The indoor temperature dropped from 15:00 to 17:00, and the interior active window was closed to minimize the loss of heat.

In order to evaluate whether the distribution of the indoor thermal environment was uniform, the difference between the maximum and minimum values of the temperature at each measurement point at each moment was calculated, the maximum temperature difference is shown in Table 3.

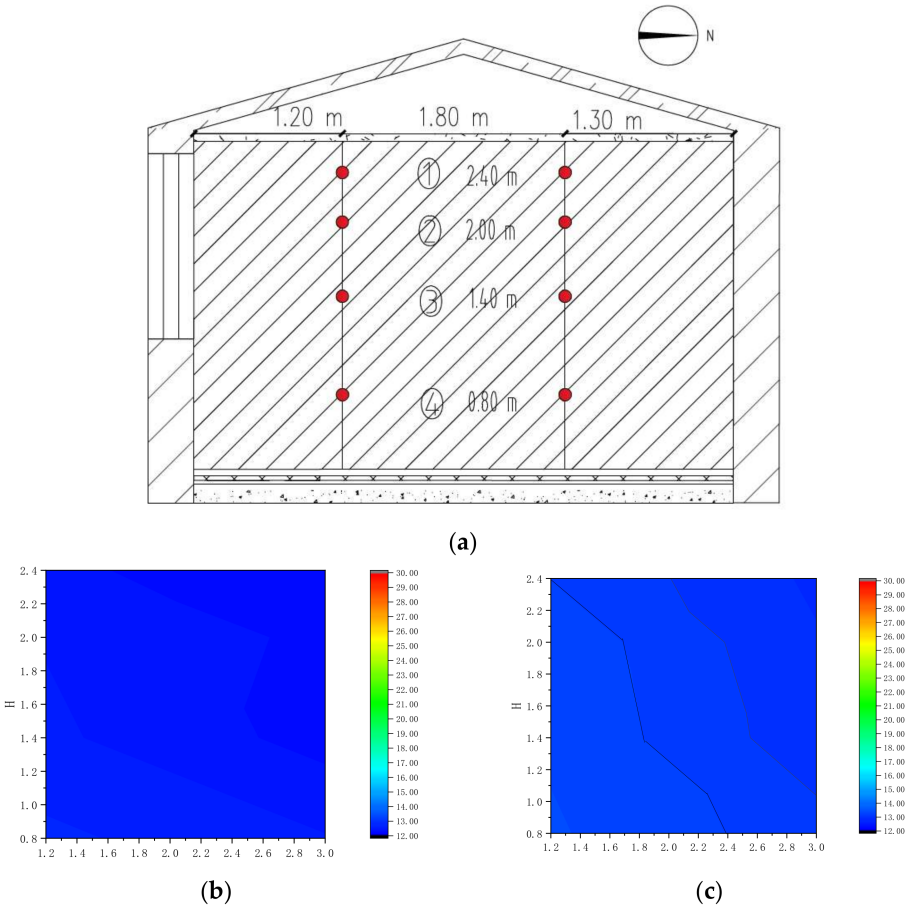


Figure 13. *Cont.*

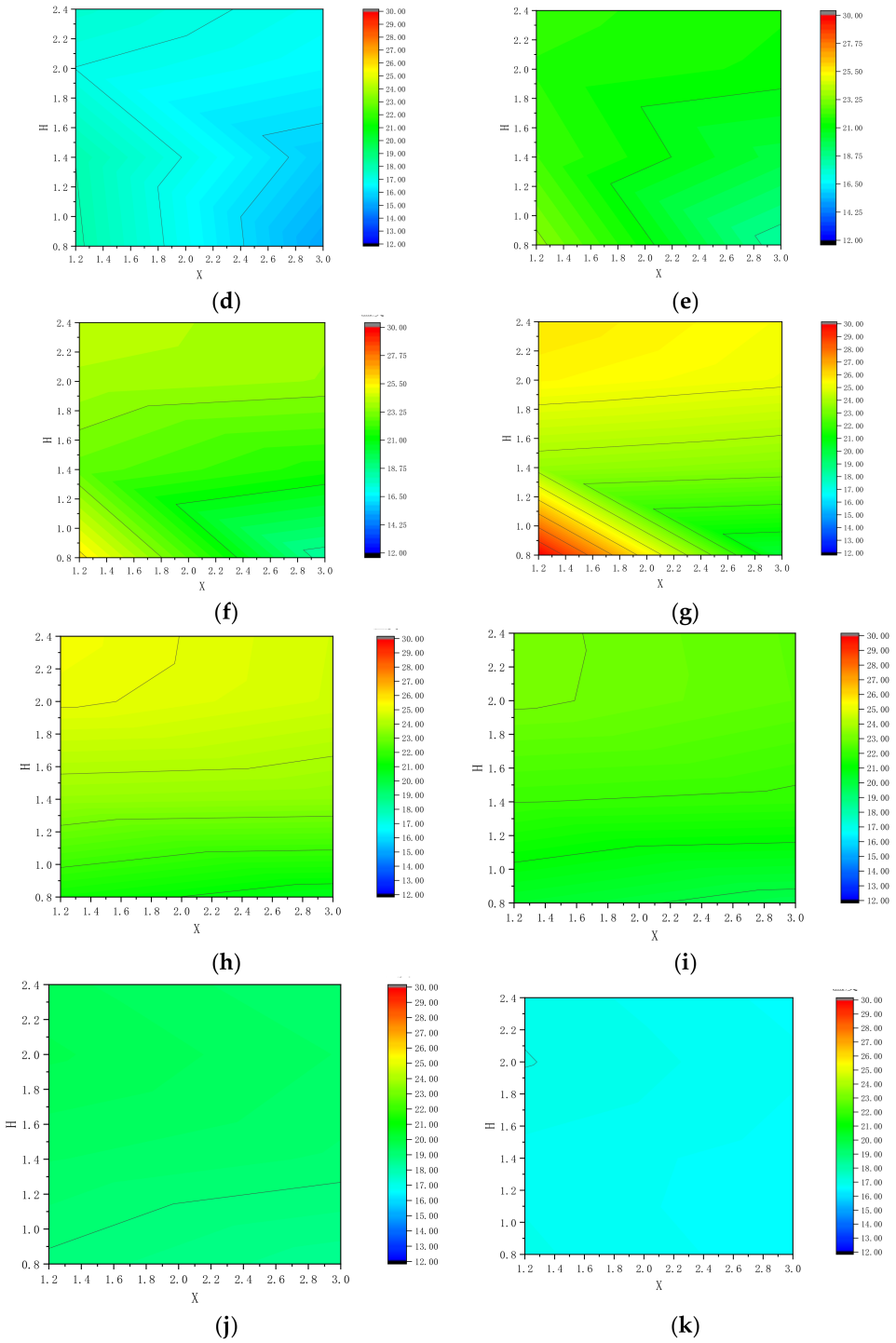


Figure 13. Tangential distribution map of indoor daytime temperature gradient on 28 January; (**a**) Indoor tangential section of temperature field; (**b**) Distribution of temperature field at 9:00; (**c**) Distribution of temperature field at 10:00; (**d**) Distribution of temperature field at 11:00; (**e**) Distribution of temperature field at 12:00; (**f**) Distribution of temperature field at 13:00. (**g**) Distribution of temperature field at 14:00; (**h**) Distribution of temperature field at 15:00. (**i**) Distribution of temperature field at 16:00; (**j**) Distribution of temperature field at 17:00; (**k**) Distribution of a temperature field at 18:00.

Table 3. Details of measurement instruments.

Time	Maximum Temperature Difference (°C)	Position
9:00	0.48	S4 and N1
10:00	0.55	S4 and N1
11:00	3.10	S1 and N1
12:00	5.13	S1 and N1
13:00	7.36	S1 and N1
14:00	9.77	S1 and N1
15:00	4.66	S1 and N4
16:00	3.42	S1 and N4
17:00	1.17	S2 and N4
18:00	0.45	S2 and N4

During the period (11:00–17:00) when the interior active window was opened, the average value of the greatest temperature differential at each measuring point at each time was 4.95 °C. From 11:00 to 14:00, the temperature differential of the lower layer in the south and north was the greatest value at each measuring location. From 15:00 to 17:00, the temperature differential of the lowest layer in the south and the highest layer in the north is the greatest value at each measuring location. The maximum temperature differential appeared at 14:00, which was 9.77 °C. During the period (9:00~10:00; 18:00) when the interior active window was closed, the average maximum temperature differential at each measuring point was 0.50 °C. As analyzed above, the indoor thermal environment is closely related to whether the interior active window is opened. When the window is closed, the difference in indoor temperature can be ignored. When the window is opened and the heating effect is significant, the interior temperature distribution is proportional to the distance from the active interior window, and the temperature difference is considerable; When the heating is diminished, the indoor temperature difference is primarily in the longitudinal distribution, with a modest temperature differential. The temperature difference percentage (D_t) is used to determine if the indoor temperature distribution is uniform. The smaller value of temperature difference percentage means the more evenly distributed indoor thermal environment. The formulas are shown in Equation (3).

$$D_t = \frac{T_\mathrm{d}}{T} \times 100\% \tag{3}$$

where D_t is the temperature difference percentage, and T_d is the temperature difference, °C; T is the average temperature, °C.

The average maximum temperature differential to the average temperature during active interior window is opened on this day is 23%. The average maximum temperature differential of reference [25] is close to 50%. This demonstrates the uniform thermal environment provided to the room by the heating through the active interior window Indicating that passive heating of the attached sunspace through the active interior window can provide a thermal environment with relatively uniform temperature distribution and meet the normal production and living needs of rural residents.

3.3. Heating Effects throughout the Winter

3.3.1. Heating Assurance Rate

This study used the TRNSYS model confirmed above and local recorded meteorological data from 1 November 2020 to 31 March 2021 to simulate the heating effect of the farmhouse with attached sunspace under zero-state response control strategy. The simulation results can be seen in Figure 14.

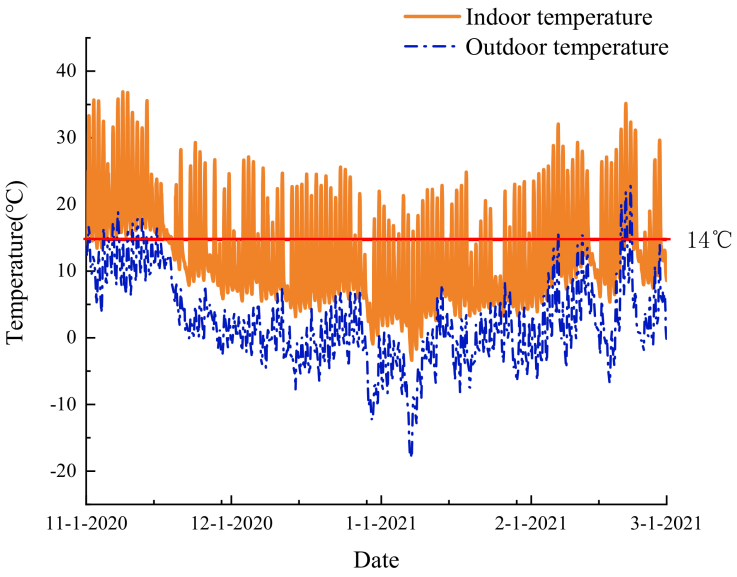


Figure 14. The simulated heating effect under the zero-state response control strategy in the winter of 2020–2021.

As shown in Figure 14, the annual minimum indoor temperature is −3.37 °C, which occurred at 7:00 a.m. on 7 January 2021, the outdoor temperature was −17.9 °C at this time, and the attached sunspace's temperature was −8.32 °C. The maximum temperature was 40.58 °C on 8 November 2020 at 13:00 p.m., and the external temperature was 13.8 °C, while the attached sunspace's temperature was 48.72 °C at this time. During the heating season, the average indoor temperature is 12.68 °C, and the hours when the internal temperature of a farmhouse is higher than 14 °C is 1094 h, accounting for 37.99% of the total hours; the average daytime temperature (8:00~17:00) is 17.75 °C, and the internal temperature of a farmhouse is greater than 14 °C for 792 h, accounting for 73.33% of the total daytime hours. According to the above statistics, under the zero-state response control strategy, the farmhouse with attached sunspace can completely rely on passive heating to maintain the indoor environment of the farmhouse higher than 14 °C for a long time. Especially during most of the daytime through the heating season, the inside temperature can be almost entirely provided by the attached sunspace's passive heating. This demonstrates the attached sunspace's excellent passive heating performance when using the zero-state response control strategy.

3.3.2. Energy-Saving Efficiency

In order to accurately evaluate the energy-saving efficiency of the attached sunspace throughout the heating season under the zero-state response control strategy and according to China's rural residential building energy efficiency design standards [26], the indoor heating temperature of the farmhouse was set to 14 °C, and the measured weather data from 1 November 2020 to 31 March 2021 were used. With the help of TRNSYS simulation software, the three scenes, including the heating energy consumption of a farmhouse with attached sunspace under the zero-state response control strategy, the heating energy consumption of farmhouse with attached sunspace but not under the zero-state response control strategy, and the heating energy of farmhouse without attached sunspace, were analyzed respectively. The simulated energy consumption result is shown in Figure 15.

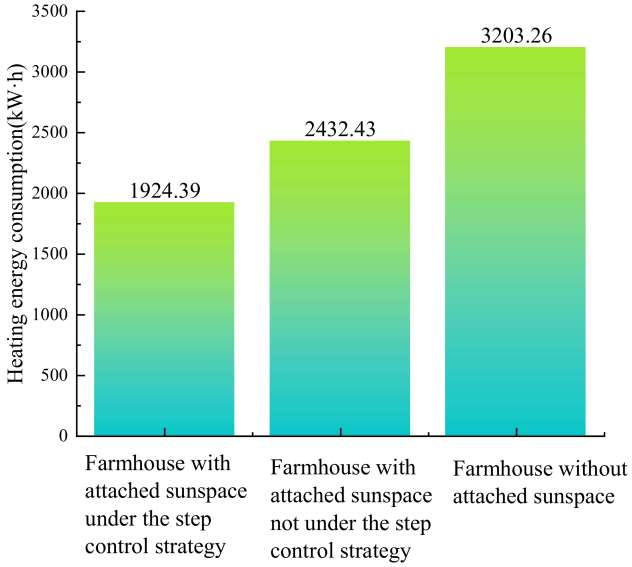


Figure 15. Energy consumption of farmhouse in heating season under different operating modes.

As demonstrated in Equation (4), attached sunspace energy-saving efficiency (ESF) can accurately measure the operation effect of passive solar farm homes [27].

$$\mathrm{ESF} = 1 - \frac{Q_1}{Q} \tag{4}$$

where Q_1 is the farmhouse with attached sunspace's heating energy consumption, kW·h; and Q is the original heating room's heating energy consumption, kW·h.

Figure 15 shows that in the heating season 2020–2021, the total energy consumption required to maintain the overall indoor temperature of 14 °C is 1924.39 kW·h if an attached sunspace is installed and under the zero-state response control strategy in the farmhouse. The total heating energy consumption of a farmhouse with an attached sunspace under the zero-state response control strategy is 2432.43 kW h. A farmhouse's total heating energy consumption required without attached sunspace is 3203.26 kW·h. In comparison to a farmhouse without an attached sunspace, the heating energy-saving efficiency of the farmhouse with attached sunspace but not under the zero-state response control strategy is 24.06%, and the heating energy-saving efficiency of the farmhouse with attached sunspace under the zero-state response control strategy is 39.92%; in comparison to the heating energy consumption of the farmhouse with attached sunspace but not under the zero-state response control strategy, the heating energy-saving rate of the farmhouse with attached sunspace under the zero-state response control strategy is 20.88%. As can be observed, the attached sunspace plays a significant role in the heating energy saving of a farmhouse and the zero-state response control strategy may further enhance the heating energy-saving efficiency in the attached sunspace while also lowering the auxiliary heat source's energy consumption and heating operation costs.

3.3.3. Carbon Emission Reduction

Carbon emission reduction G_c [28] can effectively assess the environmental benefits of passive heating in an additional sunlight room, as described in Equation (5):

$$G_c = \frac{(Q - Q_1) \times 3600}{\theta \times \eta} \times \varphi \tag{5}$$

where θ is the calorific value of standard coal, which is 29,307.6 kJ/kg; η is the combustion efficiency of heating coal, which is 0.7; φ is the carbon emission reduction per unit of

standard coal, t/t, according to the recommended value of the Energy Research Institute of the Chinese Development and Reform Commission, take 0.67 kg/kg.

Compared with the farmhouse without attached sunspace, the carbon emission reduction of the farmhouse with attached sunspace but not under the zero-state response control strategy reached 59.73 kg, and the carbon emission reduction amount of the farmhouse with attached sunspace under the zero-state response control strategy reached 90.63 kg. Compared with the farmhouse with attached sunspace under the zero-state response control strategy's carbon emission reduction, when the zero-state response control strategy is adopted, the carbon emission reduction in the attached sunspace can be increased further by 51.73%. This phenomenon shows that the use of the zero-state response control strategy can greatly reduce the carbon emissions from the operation of the auxiliary heat source of the farmhouse with attached sunspace.

4. Discussion

The application of passive heating of an attached sunspace plays an important role in carbon reduction of the rural building, particularly in the development of China's 'carbon peaking and carbon neutralization'. When solar radiation is intensive, the attached sunspace has an excellent heat collection and heating effect. It can create a satisfying indoor thermal environment under the zero-state response control strategy during the daytime. Due to the excellent insulating properties, the indoor temperature can be maintained for a portion of the time when solar radiation is weak. Such excellent passive heating performance can effectively reduce winter heating energy consumption after a large-scale promotion, and reduce carbon dioxide emissions and environmental pollution caused by heating [27].

In conventional ASPSHS, the attached sunspace serves as a well-performing heat collection component during daytime, and most of the heat is transferred to the interior of the envelope to reduce heat loss at night. However, this inappropriate control logic affects the heat utilization. The optimum zero-state response control strategy for controlling the interior active window opening time increases the heat transfer impact of the attached sunspace to the room and raises the average indoor temperature above the external temperature of 25.45 °C during the daytime. Furthermore, the influence of the pressure differential between attached sunspace and room encourages natural convection heat exchange, and the average interior temperature difference unevenness is only 23%, indicating a uniform thermal environment.

The test of the thermal environment, which immediately reflects the distribution of temperature in the attached sunspace and room, is a unique element of this experiment. According to the air temperature distribution inside the attached sunspace, the optimum place for the interior active window is in the top middle of the west-facing wall. According to the distribution of indoor temperature, the indoor thermal environment is closely related to the position of the interior active window at a distance.

The natural ventilation model with the attached sunspace and room can only more correctly mimic the average temperature, as the distribution of the temperature field is difficult to simulate. The temperature and velocity fields can be further simulated using ANSYS [29] and other tools in the following study to enable better control and design optimization of the ASPSHS.

Passive heating is challenging to achieve most of the night and exceptionally difficult during daytimes. The room's heating needs can only be satisfied by auxiliary heat sources or other forms of active heating in these hostile climates. Furthermore, due to the attached sunspace's great heat collecting ability when the solar radiation is intensive, it may bring an excessively high temperature to the inside thermal environment. If some heat storage structures can store the excess heat at this time and are paired with a wider range of control mechanisms, the attached sunspace's passive heating time can be extended, the solar heating guarantee rate can be increased, and the peaks and valleys can be retarded, resulting in a more stable indoor thermal environment.

5. Conclusions

The ASPSHS under the zero-state response control strategy can effectively improve the indoor thermal environment of farmhouses, reduce operating energy consumption and carbon emissions. The main research conclusions of this paper are as follows:

(1) The temperature difference of an attached sunspace with a room provides power for passive heating. The zero-state response control strategy of the interior active window should be related to the temperature difference. The temperature difference is about 10 °C, which can provide better heating effect.

(2) During the day, an attached sunspace's passive heating can offer a more suitable thermal environment for the farmhouse. When solar radiation is intensive, opening the interior active window can raise the internal temperature to an average of 25.45 °C higher than the outside, with a 23% discernible indoor average temperature differential indoor.

(3) Using an ASPSHS with a zero-state response control strategy, farmhouses in cold places can maintain an internal temperature of 14 °C for more than 37.99% of the time in winter and meet 73.33% of the daytime heating time.

(4) The farmhouse with attached sunspace under zero-state response control strategy can greatly reduce operating energy consumption and carbon emissions. Compared with a farmhouse without an attached sunspace, the energy for heating can be saved by 39.86%; compared to a farmhouse with an attached sunspace but not under the zero-state response control strategy, the energy for heating can be saved by 24.06%, and carbon emission reduction can be increased by 51.73%.

Author Contributions: Conceptualization, J.Z., S.L. and D.L.; methodology, J.Z. and D.L.; software, D.L.; validation, formal analysis, D.L.; investigation, D.L.; experiments, D.L.; data curation, D.L.; writing—original draft preparation, D.L; writing—review and editing, S.L.; visualization, D.L.; supervision, S.L.; project administration, J.Z.; funding acquisition, J.Z. All authors have read and agreed to the published version of the manuscript.

Funding: This research was funded by "National Key R&D Program of China" (Grant No.2018YFD1100700).

Institutional Review Board Statement: Not applicable.

Informed Consent Statement: Not applicable.

Data Availability Statement: Not applicable.

Conflicts of Interest: The authors declare no conflict of interest.

References

1. Chen, X.; Shuai, C.; Wu, Y.; Zhang, Y. Analysis on the carbon emission peaks of China's industrial, building, transport, and agricultural sectors. *Sci. Total Environ.* **2020**, *709*, 135768. [CrossRef] [PubMed]
2. Jiang, Y.; Hu, S. Paths to carbon neutrality in China's building sector. *Heat. Vent. Air Cond.* **2021**, *51*, 1–13.
3. Albayyaa, H.; Hagare, D.; Saha, S. Energy conservation in residential buildings by incorporating Passive Solar and Energy Efficiency Design Strategies and higher thermal mass. *Energy Build.* **2019**, *182*, 205–213. [CrossRef]
4. Yang, J.; Liu, Y.; Chen, Y.; Li, Y.; Zhou, Y. Research of climate regions division for applicable passive solar heating technology selection. *Acta Energ. Sol. Sin.* **2021**, *42*, 234–242.
5. Wang, D.; Liu, Y.; Jiang, J.; Liu, J. The Optimized Matching of Passive Solar Energy supply and Classroom Thermal Demand of Rural Primary and Secondary School in Northwest China. *Procedia Eng.* **2015**, *121*, 1089–1095. [CrossRef]
6. Finocchiaro, L.; Georges, L.; Hestnes, A.G. 6 Passive solar space heating. In *Advances in Solar Heating and Cooling*; Wang, R.Z., Ge, T.S., Eds.; Woodhead Publishing: Cambridge, MA, USA, 2016; pp. 95–116.
7. Wang, D.; Hu, L.; Du, H.; Liu, Y.; Huang, J.; Xu, Y.; Liu, J. Classification, experimental assessment, modeling methods and evaluation metrics of Trombe walls. *Renew. Sustain. Energy Rev.* **2020**, *124*, 109772. [CrossRef]
8. Si, P.; Lv, Y.; Rong, X.; Shi, L.; Yan, J.; Wang, X. An innovative building envelope with variable thermal performance for passive heating systems. *Appl. Energy* **2020**, *269*, 115175. [CrossRef]
9. Gong, Q.; Kou, F.; Sun, X.; Zou, Y.; Mo, J.; Wang, X. Towards zero energy buildings: A novel passive solar house integrated with flat gravity-assisted heat pipes. *Appl. Energy* **2022**, *306*, 117981. [CrossRef]

10. Zhang, L.; Ju, X.; Zeng, Y. Interpretation of "Technical Specifications for Passive Solar Buildings". *Constr. Sci. Technol.* 2012, pp. 50–54, 57. Available online: http://www.doczj.com/doc/31beb373667d27284b73f242336c1eb91a3733de.html (accessed on 19 November 2021).
11. Huo, H.; Xu, W.; Li, A. Comparison and analysis of envelope structure retrofitting schemes for rural residential building in northern china based on entropy method. *Build. Sci.* **2019**, *35*, 57–64.
12. Liu, Z.; Wu, D.; He, B.-J.; Wang, Q.; Yu, H.; Ma, W.; Jin, G. Evaluating potentials of passive solar heating renovation for the energy poverty alleviation of plateau areas in developing countries: A case study in rural Qinghai-Tibet Plateau, China. *Sol. Energy* **2019**, *187*, 95–107. [CrossRef]
13. Wang, W.; Yuan, M.; Li, Y.-Z.; Li, C. Numerical investigation on the impact of an on-top sunspace passive heating approach for typical rural buildings in northern China. *Sol. Energy* **2019**, *186*, 300–310. [CrossRef]
14. Ma, L.; Zhang, X.; Li, D.; Arıcı, M.; Yıldız, Ç.; Li, Q.; Zhang, S.; Jiang, W. Influence of sunspace on energy consumption of rural residential buildings. *Sol. Energy* **2020**, *211*, 336–344. [CrossRef]
15. Lu, S.; Tong, H.; Pang, B. Study on the coupling heating system of floor radiation and sunspace based on energy storage technology. *Energy Build.* **2018**, *159*, 441–453. [CrossRef]
16. Li, Q.; Wang, Y.; Ma, L.; Arıcı, M.; Li, D.; Yıldız, Ç. Effect of sunspace and PCM louver combination on the energy saving of rural residences: Case study in a severe cold region of China. *Sustain. Energy Technol. Assess.* **2021**, *45*, 101126. [CrossRef]
17. Zhou, Y.; Wang, D.; Liu, Y.; Liu, J. Diffuse solar radiation models for different climate zones in China: Model evaluation and general model development. *Energy Convers. Manag.* **2019**, *185*, 518–536. [CrossRef]
18. Liu, Y.; Liu, T.; Ye, S.; Liu, Y. Cost-benefit analysis for Energy Efficiency Retrofit of existing buildings: A case study in China. *J. Clean. Prod.* **2018**, *177*, 493–506. [CrossRef]
19. Jing, Z.; Jiayu, L. Study on heat transfer delay of exposed capillary ceiling radiant panels (E-CCRP) system based on CFD method. *Build. Environ.* **2020**, *180*, 106982. [CrossRef]
20. Baglivo, C.; Mazzeo, D.; Panico, S.; Bonuso, S.; Matera, N.; Congedo, P.M.; Oliveti, G. Data from a dynamic simulation in a free-floating and continuous regime of a solar greenhouse modelled in TRNSYS 17 considering simultaneously different thermal phenomena. *Data Brief* **2020**, *33*, 106339. [CrossRef]
21. Solar Energy Laboratory. *TRNSYS Version User Manual and Documentation*; University of Wisconsin: Madison, WI, USA, 2014; pp. 25–60.
22. *AG. 14-2014.*; Measurement of Energy and Demand Savings. American Society of Heating, Refrigerating and Air-Conditioning Engineers Inc.: Atlanta, GA, USA, 2014.
23. Lu, S.; Zhao, Y.; Fang, K.; Li, Y.; Sun, P. Establishment and experimental verification of TRNSYS model for PCM floor coupled with solar water heating system. *Energy Build.* **2017**, *140*, 245–260. [CrossRef]
24. Recknagel, H.; Sprenger, E.; Schramek, E. *Taschenbuch für Heizung und Klimatechnik*, 75th ed.; Oldenburg Industrieverlag: München, Germany, 2011.
25. Liu, Z.; Wu, D.; Yu, H.; Ma, W.; Jin, G. Field Measurement and Numerical Simulation of Combined Solar Heating Operation Modes for Domestic Buildings Based on the Qinghai–Tibetan Plateau Case. *Energy Build.* **2018**, *167*, 312–321. [CrossRef]
26. *GB/T 50824-2013*; Energy-Saving Design Standard for Rural Residential Buildings. CN-GB: Beijing, China, 2013.
27. Chen, M.; Shi, Y.; Liu, X. Heating study of passive solar house with sunspace. *Acta Energ. Sol. Sin.* **2012**, *33*, 944–947.
28. Zhang, X.; Xu, J.; Zhang, X.; Li, Y. Life cycle carbon emission reduction potential of a new steel-bamboo composite frame structure for residential houses. *J. Build. Eng.* **2021**, *39*, 102295. [CrossRef]
29. Lu, S.; Zhai, X.; Gao, J.; Wang, R. Performance Optimization and Experimental Analysis of a Novel Low-Temperature Latent Heat Thermal Energy Storage Device. *Energy* **2021**, *12*, 2496. [CrossRef]